RESEARCH ARTICLE SUMMARY

MOLECULAR BIOLOGY

A pathway for mitotic chromosome formation

Johan H. Gibcus,* Kumiko Samejima,* Anton Goloborodko,* Itaru Samejima, Natalia Naumova, Johannes Nuebler, Masato T. Kanemaki, Linfeng Xie, James R. Paulson, William C. Earnshaw,† Leonid A. Mirny,† Job Dekker†

INTRODUCTION: During mitosis, cells compact their chromosomes into dense rod-shaped structures to ensure their reliable transmission to daughter cells. Our work explores how cells achieve this compaction. We integrate genetic, genomic, and computational approaches to characterize the key steps in mitotic chromosome formation from the G_2 nucleus to metaphase, and we identify roles of specific molecular machines, condensin I and II, in these major conformational transitions.

RATIONALE: We used chicken DT-40 cells expressing an analog-sensitive CDK1 to produce cell cultures that synchronously enter mitosis. We collected cells at key time points during mitotic entry; analyzed chromosome organization by microscopy, chromosome conformation capture, and polymer simulations; and delineated a pathway of mitotic chromosome formation. We used engineered cell lines to study the function of condensin complexes, which are critical for mitotic chromosome formation. We fused condensin I and II subunits to plant auxin-inducible degron domains, thus enabling their rapid depletion in late G_2 just before mitotic entry. These cell lines allowed us to determine the roles of condensin I and II in specific steps of the mitotic chromosome morphogenesis pathway.

RESULTS: Our analysis of G_2 chromosomes reveals hallmarks of interphase chromosomes, including topologically associating domains and compartments. Upon entry into prophase, this organization is lost within minutes, and by late prophase, chromosomes are folded as arrays of consecutive loops condensed around a central axis. These loops project with random but mutually correlated angles from the axis. During prometaphase, the loop array undergoes two major reorganizations. First, it acquires a helical arrangement of loops. Polymer simulations of Hi-C data show that the centrally located axis acquires a helical twist so that consecutive loops emanate as the steps of a spiral staircase. Second, the chromatin loops become nested with ~400-kb outer loops split up by ~80-kb inner loops. As prometaphase proceeds, chromosomes shorten through progressive helical winding, with the numbers of loops per turn increasing. As a result, the size of a helical turn grows from ~3 Mb (~40 loops) to ~12 Mb (~150 loops). Depletion of condensin I or II before mitotic entry revealed their differing roles in mitotic chromosome formation. Either condensin can mediate loop array formation. However, condensin II is required for the helical twisting of the scaffold from which loops emanate, whereas condensin I modulates the size and arrangement of nested inner loops.

CONCLUSION: We describe a pathway of mitotic chromosome folding that unifies many previous observations. In prophase, condensins mediate the loss of interphase organization and the formation of arrays of consecutive loops. In prometaphase, chromosomes adopt a spiral staircase–like structure with a helically arranged axial scaffold of condensin II at the bases of chromatin loops. The condensin II loops are further compacted by condensin I into clusters of smaller nested loops that are additionally collapsed by chromatin-to-chromatin attractions. The combination of nested loops distributed around a helically twisted axis plus dense chromatin packing achieves the 10,000-fold compaction of chromatin into linearly organized chromosomes that is required for accurate chromosome segregation when cells divide. ∎
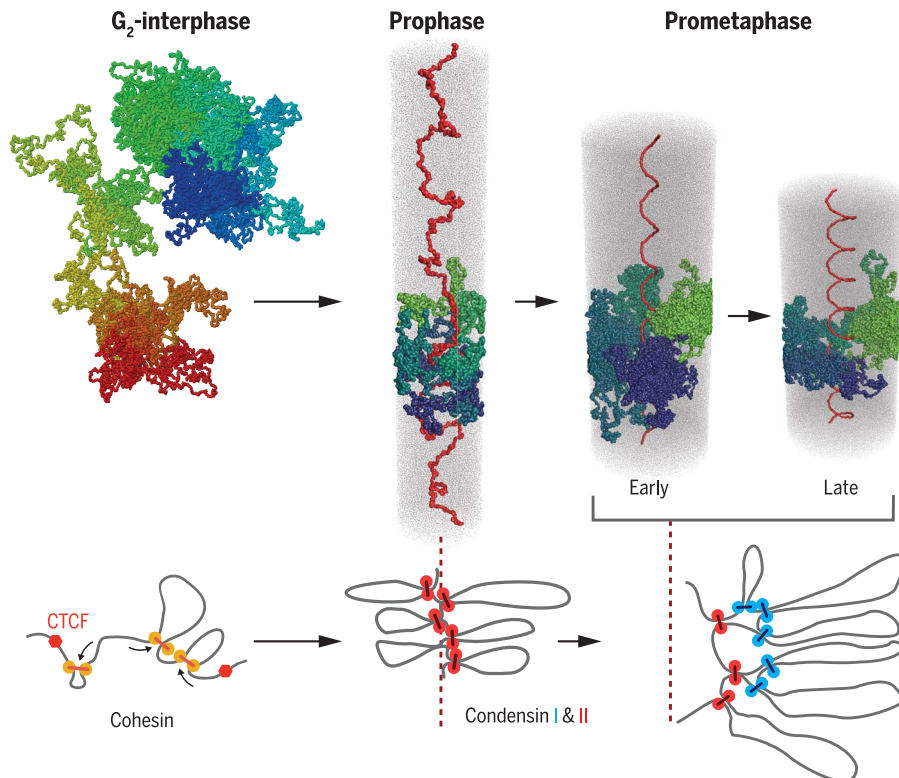
A pathway for mitotic chromosome formation. In prophase, condensins mediate the loss of interphase chromosome conformation, and loop arrays are formed. In prometaphase, the combined action of condensin I (blue spheres in the bottom diagram) and II (red spheres) results in helically arranged nested loop arrays.

RESEARCH ARTICLE

MOLECULAR BIOLOGY

A pathway for mitotic chromosome formation

Johan H. Gibcus,[1]* Kumiko Samejima,[2]* Anton Goloborodko,[3]* Itaru Samejima,[2] Natalia Naumova,[1] Johannes Nuebler,[3] Masato T. Kanemaki,[4] Linfeng Xie,[5] James R. Paulson,[5] William C. Earnshaw,[2]† Leonid A. Mirny,[3]† Job Dekker[1,6]†

Mitotic chromosomes fold as compact arrays of chromatin loops. To identify the pathway of mitotic chromosome formation, we combined imaging and Hi-C analysis of synchronous DT40 cell cultures with polymer simulations. Here we show that in prophase, the interphase organization is rapidly lost in a condensin-dependent manner, and arrays of consecutive 60-kilobase (kb) loops are formed. During prometaphase, ~80-kb inner loops are nested within ~400-kb outer loops. The loop array acquires a helical arrangement with consecutive loops emanating from a central "spiral staircase" condensin scaffold. The size of helical turns progressively increases to ~12 megabases during prometaphase. Acute depletion of condensin I or II shows that nested loops form by differential action of the two condensins, whereas condensin II is required for helical winding.

C hromosomes substantially change their conformation as cells progress through the cell cycle. Throughout most of interphase, chromosomes of vertebrates display two layers of organization: topologically associating domains (TADs) (1, 2) and A and B compartments (3). At a finer scale, chromatin looping between promoters, enhancers, and CTCF-bound sites (4, 5) facilitates gene regulation. During mitosis, these features disappear and chromosomes are compacted into dense arrays of randomly positioned consecutive chromatin loops (6–9).

Although the organization of these two states is now increasingly understood, much less is known about how cells convert from one state to the other. Previous microscopy observations revealed that chromosomes become recognizable during prophase and form linearly organized structures where sister chromatids are initially mixed (10–13). By late prophase, sister chromatid arms separate, and each chromatid is thought to be organized as an array of loops that emanate from an axial core containing condensin complexes and topoisomerase II alpha (14–18). During prometaphase, the chromatids shorten and become thicker (11), ultimately forming fully condensed metaphase chromosomes (19). How compaction of loop arrays occurs during prometaphase is not known.

We employed a chemical-genetic system for highly synchronous entry of DT40 cells into prophase. DT40 cells are karyotypically stable, near diploid (fig. S1), and have been extensively used for analysis of mitotic chromosome organization (20). The use of chemical genetics (21) in this cell system allowed us to apply the Hi-C method with high temporal resolution and to determine how chromosome conformation changes as cells disassemble the interphase nucleus and form mitotic chromosomes (22, 23). These data, combined with polymer simulations (24, 25) and direct imaging, reveal a mitotic chromosome morphogenesis pathway with distinct transitions, including compartment and TAD loss, loop array formation by late prophase, and chromosome shortening during prometaphase through growing and winding of loops around a central helical scaffold. We used an auxin-inducible degron approach (26, 27) to identify distinct key roles for condensin I and II in this pathway.

Results

Synchronous progression into mitosis

To obtain cultures of cells that synchronously enter mitosis, we arrested cells in G_2 by selectively inhibiting CDK1. We stably expressed a variant of *Xenopus laevis* CDK1 cDNA (CDK1as) harboring a Phe[80]→Gly[80] mutation in DT40 cells (22, 28). This mutation renders CDK1as sensitive to inhibition by the adenosine triphosphate analog 1NM-PP1 (22). We then used CRISPR-Cas9 to disrupt the endogenous CDK1 gene. Growing cells for 10 hours in the presence of 1NM-PP1 efficiently

arrested >90% of cells in G_2, as indicated by fluorescence-activated cell sorting (FACS) (table S1 and fig. S2) and microscopy analysis of chromosome and nuclear morphology (Fig. 1A). Washing out 1NM-PP1 led to rapid release of cells from the G_2 arrest and synchronous entry into prophase.

This system allowed us to study chromosome morphogenesis by harvesting cells at sequential time points for imaging and Hi-C analysis as they synchronously progress through mitosis. For some cultures collected at later time points (30 to 60 min), we added nocodazole 30 min before their release from the 1NM-PP1 arrest, to block the metaphase-anaphase transition (see supplementary materials and methods). All of the time courses described here were performed in duplicate and results were highly concordant. DAPI (4′,6-diamidino-2-phenylindole) staining showed the expected chromosome condensation and individualization in prophase (Fig. 1A). Nuclear envelope breakdown (NEBD) occurred around time t = ~7 to 10 min, as evidenced by staining for lamin B1, which diffuses into the cytoplasm upon NEBD (fig. S3) (29), and by measuring the association of previously cytoplasmic condensin I subunits with the chromosomes (CAP-D2, CAP-G, and CAP-H and increased levels of SMC2 and SMC4) (fig. S4, A and B). In accordance with previous studies, our proteomic analysis (fig. S4B) showed that by late prophase, cohesin (SMC1 and SMC3) has largely dissociated from the arms of sister chromatids, which separate but remain aligned (11, 12, 30, 31). Chromosome shortening subsequently occurred during prometaphase, and, at the late time points, fully condensed chromosomes were observed (Fig. 1A).

Loss of compartments and TADs in prophase

Hi-C analysis showed that G_2-arrested cells displayed all features characteristic of vertebrate interphase cells (8). First, chromosomes formed territories, as indicated by relatively high levels of intrachromosomal interactions (3). Second, chromosomes displayed the characteristic pattern of active A and inactive B compartments, as revealed by the plaid pattern of Hi-C interactions (3) (Fig. 1B). The locations of these compartments in G_2 resembled those detected in exponentially growing cells, though the compartment signal strength was stronger and the pattern sharper in the synchronous cells, likely as a result of uniformity in cell cycle stage. Third, TADs were readily visible in the Hi-C interaction maps as squares of relatively high interaction frequencies along the diagonal (Fig. 1C). TAD boundaries were similar in position and strength to those in nonsynchronous cells, as determined using an insulation score calculated from a 250-kb sliding window (32) (fig. S5). Finally, we analyzed how contact frequency (P) between locus pairs depends on their genomic distance (s). $P(s)$ decays with genomic distance, and this relationship changes with different cell cycle stages (8). For G_2 cells, we found $P(s)$ to be highly similar to that observed previously in nonsynchronous cells (figs. S6 and S7). Together, these analyses show that

[1]Program in Systems Biology, Department of Biochemistry and Molecular Pharmacology, University of Massachusetts Medical School, 368 Plantation Street, Worcester, MA 01605, USA. [2]Wellcome Centre for Cell Biology, University of Edinburgh, King's Buildings, Max Born Crescent, Edinburgh EH9 3BF, Scotland, UK. [3]Institute for Medical Engineering and Science and Department of Physics, Massachusetts Institute of Technology, Cambridge, MA 02139, USA. [4]Division of Molecular Cell Engineering, National Institute of Genetics, Research Organization of Information and Systems, and Department of Genetics, SOKENDAI, Yata 1111, Mishima, Shizuoka 411-8540, Japan. [5]Department of Chemistry, University of Wisconsin Oshkosh, 800 Algoma Boulevard, Oshkosh, WI 54901, USA. [6]Howard Hughes Medical Institute, University of Massachusetts Medical School, 368 Plantation Street, Worcester, MA 01605, USA.
*These authors contributed equally to this work.
†Corresponding author. Email: bill.earnshaw@ed.ac.uk (W.C.E.); leonid@MIT.edu (L.A.M.); job.dekker@umassmed.edu (J.D.)

G_2 chromosomes, which are composed of two closely aligned and likely catenated sister chromatids, are organized similarly to G_1 chromosomes (8).

This interphase chromosomal organization was rapidly lost upon release of cells into prophase. As soon as 5 min after removal of 1NM-PP1, we detected a marked reduction in the typical plaid pattern of long-range interactions, indicating a loss of compartments (Fig. 1B). By 10 min (late prophase), compartments were mostly gone. At the same time, TADs were also lost (Fig. 1C and fig. S8).

We used eigenvector decomposition to quantify the disappearance of compartments (33). The first eigenvector readily captured compartments at $t = 0$ and 2.5 min, but starting at $t = 5$ min it explained progressively less of the variance in the Hi-C interaction maps, indicating weakening of the compartment structure. By $t = 7.5$ min, the strength of the first eigenvector fell to 17% (from 80% at $t = 0$ min), and by $t = 10$ min, it no longer captured compartments. Loss of compartments was also quantified by calculating the ratio of A-to-A or B-to-B interactions over A-to-B interactions for the full time course. From $t = 0$ to 2.5 min and onward, this fraction decreased steadily, indicating that preferential interactions within compartments are lost (Fig. 1D and fig. S9).

The strength of TADs can be quantified using the insulation score, which indicates the amount of contacts formed across a locus up to a certain distance (32). TAD boundaries have a low score (indicative of high insulation), whereas loci inside TADs show a high score (little insulation). The genome-wide variance of insulation scores provides a quantitative measure of the presence of TADs (8). Starting at $t = 2.5$ min, the variance of the insulation profiles progressively decreased, indicating the loss of TADs (Fig. 1C and fig. S5B). By $t = 7.5$ min, the variance was reduced by more than a factor of 2, and by $t = 10$ min, no TADs were detected. This conclusion was confirmed by plotting the average Hi-C interaction pattern at and around TAD boundaries identified in G_2 at different time points during mitosis (Fig. 1C). Insulation was strongest in G_2, and, by late prophase, insulation values were near background levels (quantified in fig. S10). We conclude that compartments and TADs disappear rapidly during early prophase.

By late prophase, when sister arms have resolved (11, 34), and around the time of nuclear envelope breakdown ($t \sim 7.5$ to 10 min), the Hi-C maps are characterized by a general decay of contact frequency P with genomic distance s (Fig. 2A). The shape of the $P(s)$ curve changes as prophase progresses. In G_2 cells, it is shallow [$P(s) \sim s^{-0.5}$] up to a distance of several hundred kilobases, reflecting compaction within TADs (35, 36), but for larger distances the decay becomes steeper.

During prophase, the initial shallow decay extends for longer-range interactions, with a steeper drop at 2 Mb at $t = 10$ min, which suggests a higher degree of compaction. As we demonstrate below, this decay and shape are consistent with the formation of a linearly arranged, layered organization of the chromosome (8), where the size of each layer corresponds to the position of the steep drop in the $P(s)$ curve.

Appearance of a second diagonal band in Hi-C maps from prometaphase cells

At $t = 15$ min, when cells have entered prometaphase, the Hi-C maps produce a $P(s)$ curve with a drop at 2 Mb. A distinct second diagonal band appears, running in parallel with the primary diagonal for all loci and chromosomes (Fig. 1B and fig. S11). This second diagonal represents increased interaction frequencies between any pair of loci separated by ~3 Mb. At 15 min, this feature is clearly observed in $P(s)$ plots as a local peak at ~3 Mb (Fig. 3A and figs. S6 and S7). As cells progress through prometaphase, the position of the drop in $P(s)$ and the position of the second diagonal migrate to larger genomic distances (Fig. 3A and figs. S6 and S7). By $t = 60$ min, when compact metaphase chromosomes have formed, the second diagonal is positioned at ~12 Mb and appears more diffuse. The second diagonal appears in all chromosomal maps, and
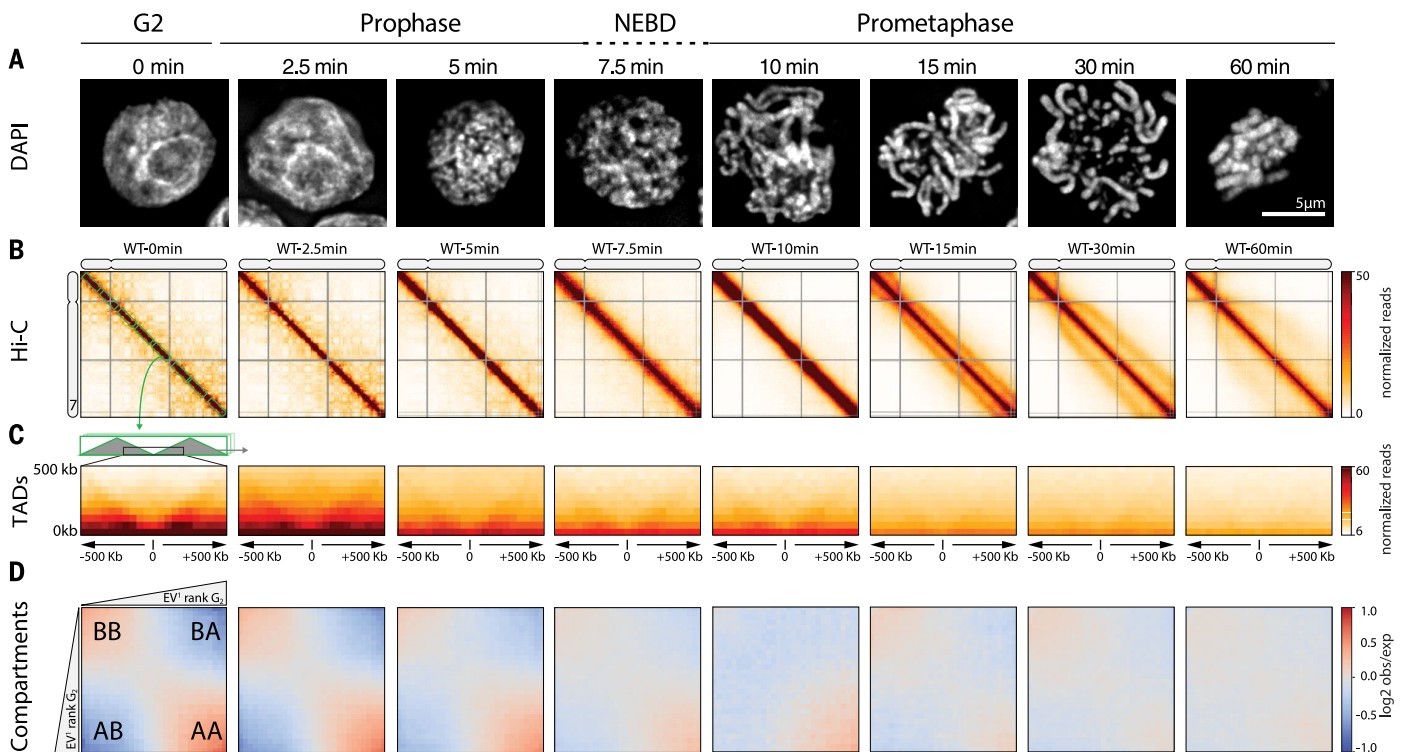
Fig. 1. Chromosome morphogenesis during synchronous mitosis.
(**A**) Representative DAPI images of nuclei and chromosomes in CDK1as DT40 cells taken at the indicated time points (in minutes) after release from 1NM-PP1–induced G_2 arrest show mitotic chromosome formation. NEBD, nuclear envelope breakdown. (**B**) Hi-C interaction maps of chromosome 7 (binned at 100 kb) from cells collected at the indicated time points in prophase and prometaphase show large-scale changes in contact frequencies as cells progress through mitosis. (**C**) The average interaction maps centered around G_2 TAD (topologically associating domain) boundaries. TAD boundaries disappear. (**D**) Compartmentalization saddle plots: average distance-normalized interaction frequencies between cis-pairs of 100-kb bins arranged by their G_2 eigenvector value (EV^1). Compartments disappear.

its position is independent of chromosome size over two orders of magnitude (fig. S11). The appearance and movement of the second diagonal is not dependent or affected by nocodazole: No nocodazole was added to the $t = 15$ min sample, and a replicate Hi-C data set obtained from a culture collected at $t = 30$ min in the absence of nocodazole was nearly identical to the data obtained in the presence of nocodazole (table S2 and figs. S7 and S8). Together, these $P(s)$ curves reveal a periodicity of interactions that reflects chromosome structure at the scale of megabases.

The only known regular periodic structural feature of chromosomes is helical coiling, which was first described in 1880 ([37]) and can be observed in certain chromosome preparations ([10, 38–40]). Experimentally induced banding of the chromosome arms is much more irregular ([41]). In helical chromosomes with a pitch (the length of a complete helical turn) of ~3 Mb, each locus is in relatively close proximity to loci positioned one turn up or down the chromosome; that is, 3 Mb up- or downstream along the DNA. The progressive movement of the second diagonal band to larger distances during prometaphase would reflect an increased "winding up" and shortening of the helix.

Although these are the first Hi-C data revealing the helical coiling of chromosomes, the chicken DT40 late prometaphase ($t = 60$ min) Hi-C contact maps strongly resemble those for mitotic human HeLa S3 chromosomes that we had re-ported earlier ([8]). In fact, reanalysis of mitotic HeLa S3 Hi-C data in more detail by deeper sequencing revealed a weak second diagonal band at a ~10-Mb distance (fig. S12), which suggests that this periodic folding is a conserved feature of vertebrate mitotic chromosomes.

Testing models of chromosomes

Previous studies have suggested that mitotic chromosomes are organized as arrays of consecutive loops emanating from a condensin-rich scaffold, forming a polymer bottlebrush ([42, 43]), with a layered organization of loops ([6, 8, 19, 44]). To understand chromosome organization at different stages of compaction, we built coarse-grained models of chromosomes as arrays of loops,
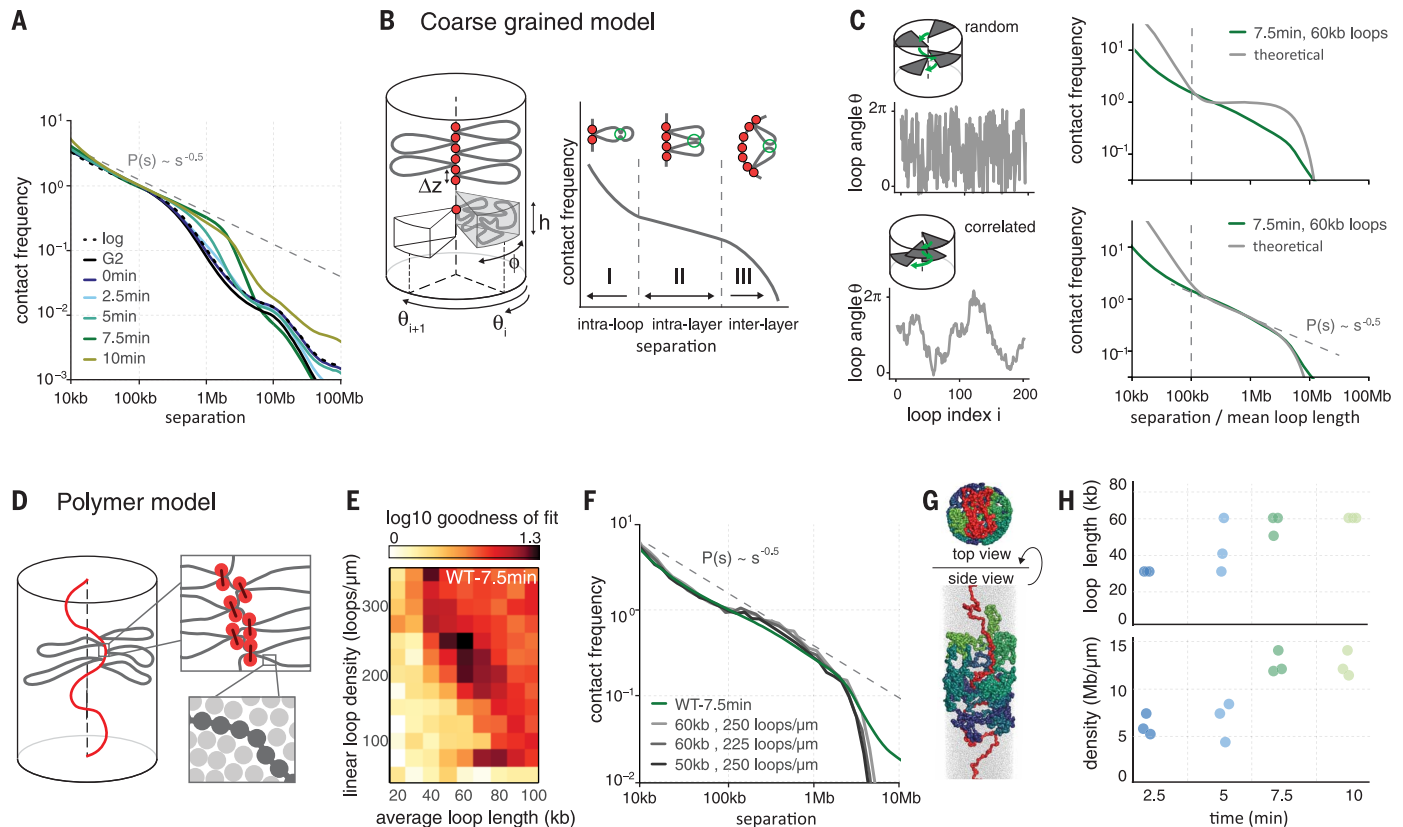
Fig. 2. Prophase chromosomes fold as axially compressed loop arrays.
(**A**) Genome-wide curves of contact frequency $P(s)$ versus genomic distance s, normalized to unity at $s = 100$ kb. The curves are derived from prophase Hi-C data at the indicated time points after release from G_2 arrest. The dotted line indicates $P(s) = s^{-0.5}$ observed for mitotic chromosomes ([8]). log, asynchronous culture. (**B**) Overview of the coarse-grained model of prophase chromosomes. The chromosome is compacted into a series of consecutive loops and compressed into a cylindrical shape. The loop bases form a scaffold at the chromosomal axis, each loop occupies a cylindrical sector of height h and angular size φ, oriented at angle θ_i. Δz, loop separation. The coarse-grained model predicts the $P(s)$ curve to have three distinct regions: intraloop (I), intralayer (II), and interlayer (III) regions. (**C**) Best-fitting $P(s)$ predictions by the coarse-grained model for late prophase ($t = 7.5$ min) under two different assumptions on loop orientations: (top) uncorrelated and (bottom) correlated orientations of consecutive loops. Uncorrelated angular loop orientations lead to a plateau in $P(s)$ in the intralayer, whereas correlated angles lead to the experimentally observed $P(s) = s^{-0.5}$ (right panels). (**D**) Polymer models of prophase chromosomes. A chromosome is modeled by a polymer (dark gray circles), arranged into an array of consecutive loops (loop bases indicated in orange) and compacted into a cylinder with a specified volume density (bottom right). (**E**) Goodness of fit for simulated versus experimental $P(s)$. Polymer simulations were performed for a range of loop densities and loop lengths, and $P(s)$ was calculated for each simulation. The heat map shows the quality of a match between the predicted and experimental $P(s)$ curves at late prophase ($t = 7.5$ min). (**F**) $P(s)$ derived from late prophase Hi-C experiments (green line) and the best-fitting polymer models (grayscale lines). Average loop size and linear density of loops along the chromosome axis are listed. (**G**) Top and side view of the best-fitting polymer model of late prophase chromosomes. Loop bases are shown in red and several loops rendered in different colors. (**H**) Average loop size and linear density of the three best-fitting models of prophase chromosomes at different time points.

aiming to reproduce $P(s)$ curves of Hi-C data, separately for each time point. In these models, a chromosome is represented by a cylinder with an axial scaffold; loop bases are arranged consecutively along the scaffold, and each chromatin loop, emanating from the scaffold in a particular direction, is represented by a blob of loci (Fig. 2B and supplementary materials. Further support for a centrally located spiraling scaffold is provided by analysis of chromosome shape and SMC2–mAID–GFP, CAP-H–mAID–GFP, or CAP-H2–mAID–GFP localization along mitotic chromosomes from colchicine-arrested and anaphase DT40 cells (mAID, minimal auxin-inducible degron domain; GFP, green fluorescent protein) (Fig. 3B and figs. S15 and S16). We observe a pattern of condensin localization that is consistent with a helical path of the scaffold. Loops are regularly placed along the axis, with angular positions determined by a stochastic model. Loop sizes are exponentially distributed, and bases of loops are not positioned at defined genomic sequences or loci (8). Analysis of condensin chromatin immunoprecipitation (ChIP) data for DT40 cells (45) supports sequence-independent positioning for >95% of loops (fig. S13; also see Discussion section). For specific models of loop arrangements, presented below, the $P(s)$ curve can be found analytically as the return probability of a stochastic process describing angular positions of loops (supplementary materials and methods section "Coarse-grained model of contact probability decay in mitotic chromosomes"). The resulting $P(s)$ always has three regions (Fig. 2B): (i) the intraloop region at short separations, where two loci are likely to be within the same loop and $P(s)$ reflects the internal organization of loops; (ii) the intralayer region at larger genomic separations, where loci are positioned on different loops within the same axial layer of the cylindrical chromosome and $P(s)$ reflects the specific arrangement of loops relative to each other; and (iii) the interlayer that appears as a steep drop in contact frequency at large genomic distances, where loci are positioned in loops that are so distant along the scaffold that their blobs can no longer overlap. In the $P(s)$ plot of experimental Hi-C data throughout mitosis, the intralayer region and the drop-off can be readily discerned (Fig. 2, A and C).

Prophase chromosomes

The coarse-grained models show that the relative orientation of consecutive loops strongly affects the shape of the $P(s)$ curve in the intralayer region. If the orientations of consecutive loops are independent of each other, the contact frequency $P(s)$ does not decay with genomic distance in the intralayer region, as any two of loops within a layer are equally likely to interact (Fig. 2C). In contrast, introducing correlations between orientations of consecutive loops—that is, forcing neighboring loops to project in similar directions—makes them follow an angular random walk. The angular random walk is a one-dimensional random walk on a circle and has a return probability of $P(s) \sim s^{-0.5}$ until the full turn is made by the walk. The $P(s) \sim s^{-0.5}$ decay followed by a drop is in good

agreement with the late prophase Hi-C data (t = 7 to 10 min) (Fig. 2C). Taken together, these results suggest that by late prophase chromosomes are already organized into arrays of consecutive loops with correlated angular orientations.

We developed detailed polymer models to test whether specific classes of conformations can reproduce experimental Hi-C data, though our models do not prove mechanisms by which these structures form. Further, all of our simulations produce equilibrium models and do not reflect kinetics of chromosome folding. In these models, chromatin is represented as a 10-nm fiber (46, 47), where one monomer corresponds to one nucleosome (Fig. 2D), allowing us to simulate up to 40 Mb of chromatin. Prophase chromosomes are modeled as arrays of consecutive loops of exponentially distributed length and random genomic locations, emanating from a flexible scaffold, as would result from a loop extrusion process (48). The loop array is further condensed by imposing poor solvent conditions to the density observed in electron microscopy (one nucleosome per cube of dimensions 11 nm by 11 nm by 11 nm; i.e., ~40% volume fraction) (49) while preserving the overall cylindrical shape of the chromosome (Fig. 2D). We systematically varied two parameters: the average loop size and the linear loop density along the chromosomal scaffold (Fig. 2E). For all combinations, we generated equilibrium conformations, simulated a Hi-C experiment, and evaluated its ability to reproduce $P(s)$ curves from Hi-C data for different time points during prophase (Fig. 2, E to H).

These polymer models can accurately reproduce $P(s)$ (20 kb < s < 4 Mb) for all prophase time points, in agreement with the prediction of the coarse-grained model (Fig. 2C). The best-matching models for later prophase time points, when sister chromatids are separate and lie side-by-side, have gradually increasing average loop size—from 40 to 50 kb at t = 5 min to ~60 to 70 kb at t = 10 min (Fig. 2H)—thus reproducing the gradually shifting position of the drop-off from 2 to 3.5 Mb (i.e., increase of the layer size) while maintaining about the same linear loop density of ~50 loops per layer and ~250 loops per micrometer. These results are consistent with a model in which loop arrays are formed early in prophase and loop sizes grow gradually, for instance, by merging smaller adjacent loops (25). Thus, both coarse-grained models and polymer simulations indicate that by late prophase, chromosomes fold as dense arrays of loops, with consecutive loops positioned with correlated radial orientations.

Prometaphase spirals

A notable feature of prometaphase Hi-C data is the appearance of the second diagonal band, which appears as a distinct peak on the $P(s)$ curves (Fig. 3A). This feature cannot be explained by interactions between sister chromatids, as these become minimal in prometaphase, and simulations show that no amount of overlap between sisters gives rise to such a periodic pattern in interactions (fig. S14). As argued above, periodic

interactions seen by Hi-C are most readily explained by a helical organization of mitotic loop arrays, which has been observed microscopically (6, 10, 40, 50). Two classes of chromosome architecture can give rise to periodicity in contact frequencies: an external helix in which the whole chromosome is folded into a solenoid (50) (the solenoid model) and a staircase model in which consecutive loops wind in a helical order around a centrally located scaffold (internal helix). The term "scaffold" does not necessarily imply a solid integrated structure stretching from one end of the chromosome to the other. By modeling, we examined these classes of architectures and the continuum of models between them.

To explore whether an internal helix can arise through reorganization of loop orientations while preserving the cylindrical morphology of the whole chromosome, we extended our coarse-grained prophase model (Fig. 2B) by adding a preferred angular orientation for each loop: (i) As in prophase, the orientation of each loop is correlated with its neighbors; or (ii) these loops have preferred, but not fixed, orientations that follow a helical path, thus winding around the chromosomal scaffold (Fig. 3B). Loops in this spiral staircase model follow an angular Ornstein-Uhlenbeck random walk with bias toward preferred positions, and $P(s)$ can be found analytically (51) (see supplementary materials and methods, subsection "Loops with spiral staircase orientation"). This coarse-grained model yields a $P(s)$ curve that closely follows the experimental prometaphase $P(s)$ and displays both the $P(s) \sim s^{-0.5}$ decay and the narrow peak corresponding to the second diagonal band (Fig. 3C). These results indicate that (i) the emergent second diagonal band in Hi-C data can result from a spiral organization and (ii) such organization can arise from preferred orientations of loops around the central scaffold.

Detailed polymer modeling allowed us to explore a broader range of architectures, with both external and internal helices, and to obtain quantitative estimates of loop sizes and other aspects of organization. Two aspects of the prometaphase organization must be captured by any model: (i) a higher linear density of chromatin of up to 50 to 70 Mb/μm, necessitating an evolution of the loop architecture, and (ii) spiraling of the scaffold. The higher density of loops can be achieved by a nested loop organization in which several smaller (inner) loops are organized consecutively within each larger (outer) loop whose bases form the central axis (Fig. 3D). The presence of nested loops is an essential feature for prometaphase models, as models with a single layer of loops could not reproduce Hi-C $P(s)$ curves even when other parameters were varied (fig. S14B). To model helical architecture, we made the scaffold follow a helical path in three dimensions while allowing loops to adopt their equilibrium conformations within an otherwise cylindrical chromosome (Fig. 3D).

We systematically varied the model parameters, such as geometry of the spiral scaffold and loop sizes (Fig. 3E). By doing this, we were also able to probe different lengths and widths of chromosomes as the volume density was kept

constant. For t = 30 min, the best agreement was achieved for a relatively narrow internal spiral staircase–like scaffold (width R = 30 to 60 nm) (Fig. 3, F and G). This spiral is much narrower than the ~300-nm diameter of the chromatid and has a small pitch (height of one turn: 100 to 200 nm) (Fig. 3H). This spiral

arrangement of loop bases can achieve helical winding of loops that reproduces the second diagonal in the interaction maps and the peak on the $P(s)$ curves for t = 15, 30, and 60 min (Fig. 3, F to H). Wider spiraling of the scaffold (Fig. 3G, III) approximating external helix architectures (50) failed to accurately reproduce $P(s)$ (fig. S14C).

Further support for a centrally located spiraling scaffold is provided by analysis of chromosome shape and SMC2-mAID–GFP, CAP-H–mAID–GFP, or CAP-H2–mAID–GFP localization along mitotic chromosomes from colchicine-arrested and ana-phase DT40 cells (mAID, minimal auxin-inducible degron domain; GFP, green fluorescent protein)
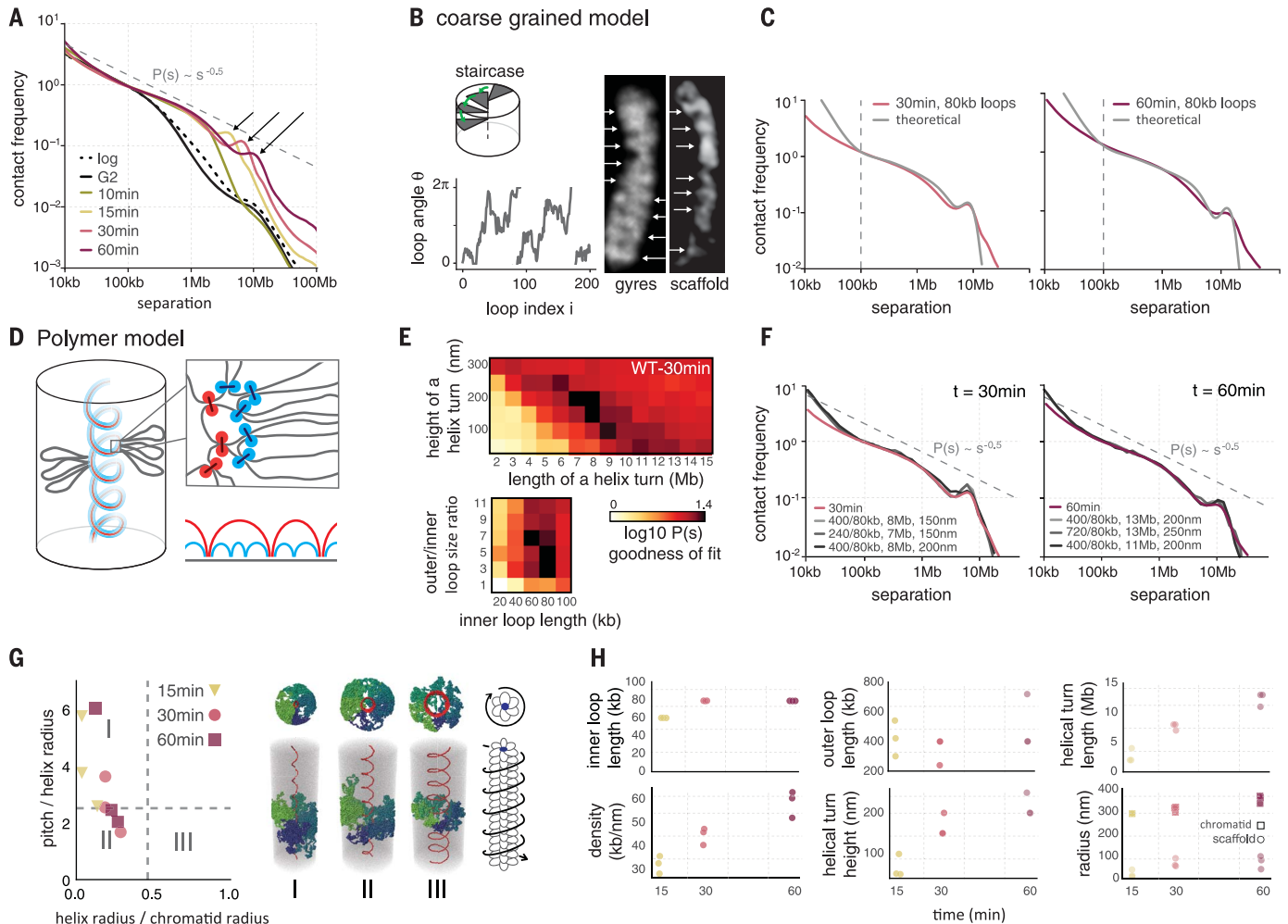
Fig. 3. Helical organization of prometaphase chromosomes. (A) Genome-wide curves of contact frequency $P(s)$ versus genomic distance (separation, s), normalized to unity at s = 100 kb. The curves are derived from Hi-C data obtained from prometaphase cells (t = 10 to 60 min after release from G2 arrest). The dashed line indicates $P(s) = s^{-0.5}$. Arrows indicate positions of a local peak in $P(s)$ representing the second diagonal band observed in Hi-C interaction maps. (B) Coarse-grained model of prometaphase chromosomes with staircase loop arrangement. (Left, top) The staircase loop arrangement implies that loops rotate in genomic order around a central scaffold (supplementary materials). (Left, bottom) Angles of adjacent loops are correlated and steadily increasing, reflecting a helical arrangement of loops. (Right) This helical arrangement can be observed as gyres by DNA staining, and a helical scaffold can be observed in cells expressing GFP-tagged condensin. (C) Best-fitting $P(s)$ predictions by the staircase coarse-grained model for late prometaphase t = 30 min (left panel) and t = 60 min (right panel) after release from G2 arrest (Hi-C data: colored lines; model; gray lines). (D) Polymer model of prometaphase chromosomes. Chromosomes are modeled as arrays of consecutive nested loops with a helical scaffold (outer loops in red; inner loops in blue; also indicated diagrammatically at bottom right). (E) Goodness of fit for simulated versus experimental $P(s)$.

Polymer simulations were performed with varying the helix height (nano-meters), the size of a helical turn (megabases), and the sizes of the inner and outer loops. $P(s)$ was calculated for each simulation. The heat maps show the quality of the best match between the predicted and experimental $P(s)$ at prometaphase (t = 30 min), when two out of four parameters were fixed to the specified values. (F) $P(s)$ derived from prometaphase Hi-C experiments (colored lines) and the best-fitting polymer models (gray lines). (Left) t = 30 min; (right) t = 60 min after release from G2 arrest. The average size of outer and inner loops, length of a helix turn, and helical pitch are indicated. (G) Parameters of the helical scaffolds from the best-fitting polymer models. x axis: ratio of the radius of the helical scaffold to that of the whole chromatid; y axis: ratio of the pitch to the helix radius. The dashed lines show the corresponding values (0.46 and 2.5122) for the optimal space-filling helix (84). Classical solenoid configurations are predicted to be in sector III, whereas the spiraling staircase configurations are in I and II. On the right, three examples of models of type I, II, and III are shown with loops bases in red and several individual loops rendered in different colors. Also shown is a schematic of a prometaphase chromosome with the helical winding of loops indicated by an arrow around the loop array. (H) Parameters of the best three models of prometaphase chromosomes at different time points.

(Fig. 3B and figs. S15 and S16). We observe a pattern of condensin localization that is consistent with a helical path of the scaffold. Taken together, coarse-grained and polymer models that agree with Hi-C data overwhelmingly support the spiral staircase (internal helix) architecture of the scaffold (I and II in Fig. 3G) and subsequent helical winding of loops.

By fitting consecutive time points probed by Hi-C, we found that the linear chromatin density of the best-matching models continued to grow throughout prometaphase, in agreement with the observed steady shortening of mitotic chromosomes (Figs. 1A and 3H and fig. S18). Simulations show that shifting the peak in $P(s)$ to larger genomic distances representing the second diagonal in consecutive time points (Fig. 3A) can be achieved by increasing the radius of the helical scaffold from 30 to 100 nm, the radius of the chromatid from 300 to 360 nm, and the pitch from 100 to 250 nm, while maintaining a constant outer and inner loop size (~400 and ~80 kb, respectively) (Fig. 3H). These changes lead to an increase in the amount of DNA (megabases) per turn of the spiral from ~3 Mb in early prometaphase up to ~12 Mb by late prometaphase. Thus, comparison of the dimensions of our best models with direct microscopic measurements of prometaphase chromosomes prepared according to the Hi-C protocol reveals good agreement between experiment and predictions (fig. S17).

Condensins are critical for prophase chromosome morphogenesis

To determine the role of condensin complexes in chromosome morphogenesis, we fused an mAID degron to SMC2 (table S3). In the presence of the plant F-box protein OsTIR1, the addition of auxin induces rapid proteasome-dependent degradation of the SMC2-mAID protein, thus disrupting both condensin I and II complexes (18, 26, 27). Incubation of cells for 3 hours in the presence of auxin during the 1NM-PP1–induced G_2 arrest (supplementary materials) reduced SMC2 levels to <5% (fig. S19). Surprisingly, this did not affect global chromosome organization, as compartments and TADs were comparable to those in wild-type (WT) G_2 arrested cells (Fig. 4A and fig. S20). Cells entered prophase rapidly after washout of 1NM-PP1, and the onset of NEBD, as indicated by DAPI staining, occurred as in the wild type at ~7 to 10 min (fig. S21).

Chromosomes in SMC2-depleted cells did not form well-resolved chromatids as cells progressed to prometaphase, confirming previous observations (fig. S21) (18, 52–54). Chromatin in such cells lacks functional condensin (55, 56) but nonetheless achieves a normal degree of chromatin compaction despite the absence of individualized chromosomes (57). FACS analysis confirmed that these cells are incapable of normal mitotic exit. They ultimately undergo mitotic slippage, forming tetraploid interphase cells (fig. S2).

Hi-C analysis revealed that in the absence of SMC2, interphase compartments and TADs were still present and largely unaffected by late prophase, at a time when they were completely dis-

assembled in the wild type (t = 10 min) (Fig. 4A and fig. S20A). NEBD and spindle assembly did occur, which indicates that cells progressed to physiological prometaphase. In prometaphase (t = 45 and 75 min), compartments and TADs progressively weakened but remained detectable (Fig. 4A and figs. S22 and S23). No second diagonal, characteristic for WT prometaphase, ever appeared in the Hi-C maps (Fig. 4A); instead $P(s)$ curves show little change from G_2 (figs. S20A and S24 to S26). Preferential compartmental (A-to-A and B-to-B) interactions became progressively weaker (figs. S20A and S22A). Analysis of the variation of the insulation score along chromosomes indicated that TAD boundaries were reduced in strength but not eliminated (Fig. 4A and fig. S23). Further, removal of cohesin (SMC1 and SMC3) and CTCF from chromatin, as assessed by chromatin enrichment for proteomics (58), was delayed and reduced compared with in the wild type (fig. S4D). This may explain the incomplete loss of TAD boundaries. Combined, these data reveal that condensin is not required for TAD and compartment architecture during interphase. In its absence, mitotic chromatin is compacted but chromosomes do not become individualized or acquire the normal mitotic morphology; however, elements of interphase architecture are partially preserved. This indicates (i) that compaction and formation of rod-shaped mitotic chromosomes are two separate processes, as assumed by our model; and (ii) condensin plays a critical role in the formation of proper morphology and internal organization of mitotic chromosomes, as well as in disassembly of the interphase architecture (59).

Condensin I and II play distinct roles in chromosome morphogenesis

Next, we separately determined the roles of condensin I and II. Condensin I and II bind chromatin independently (52, 56, 60, 61), and recent in vitro mitotic chromosome assembly experiments show that they can act individually (62). Therefore, depletion of one condensin complex is unlikely to affect the other, though we cannot rule out more subtle interplay between the complexes. We fused auxin-inducible degron domains to the condensin II–specific kleisin CAP-H2 (CAP-H2–mAID) or the condensin I–specific kleisin CAP-H (CAP-H–mAID) in CDK1as DT40 cells (supplementary materials and methods). The addition of auxin led to >95% protein depletion in G_2-arrested CAP-H–mAID or CAP-H2–mAID cells (fig. S19). Cells were then released from the G_2 block, and chromosome conformation was determined by microscopy and Hi-C as cells progressed through mitosis.

Depleting either condensin I or II alone led to less severe phenotypes than depleting both together (fig. S21). In contrast to cells lacking both condensin I and II (SMC2-mAID), these cells exited mitosis within 3 hours after entry into prophase (fig. S2).

Comparison of Hi-C interaction matrices (Fig. 4, B and C, and fig. S20, B and C) and $P(s)$ curves (Fig. 5, A and B, and figs. S24, B and C; S25; and

S26) for CAP-H– and CAP-H2–depleted cells in late prometaphase (t = 30 min and 60 min) shows that they capture different aspects of the WT architecture. The $P(s)$ curve for CAP-H2–depleted cells, where only condensin I remains active, matches that of the intralayer organization of the wild type up to ~6 Mb and lacks the second diagonal band (Fig. 5B). The $P(s)$ curve for CAP-H–depleted cells (active condensin II) matches that of the wild type only for the long-range organization (6 to 20 Mb), including the second diagonal band (Fig. 5B). CAP-H–depleted cells have a much lower contact frequency between loci separated by <6 Mb than do WT and CAP-H2–depleted cells. Thus, condensin I and II play distinct roles at different structural levels in mitotic chromosome morphogenesis, providing a mechanistic explanation for earlier microscopic studies (60, 61, 63, 64).

Helical winding during prometaphase requires condensin II

In condensin II–depleted cells, both A and B compartments and TADs were lost starting around the prophase-prometaphase transition (t = 10 to 15 min) (Fig. 4B and figs. S20 and S22). In late prometaphase (t = 30 to 60 min), chromosomes in these cells were longer and narrower than WT chromosomes, as previously observed (60, 63, 64) (fig. S21). $P(s)$ curves for t = 10 and 15 min (early prometaphase) resembled those in the wild type for late prophase (t = 10 min) (compare Fig. 5A with Fig. 2A), displaying a mild decay followed by a steep drop that is characteristic for a densely packed loop array (Fig. 2B). Most notably, CAP-H2 depletion prevented emergence of the second diagonal band in prometaphase in Hi-C contact frequency maps and $P(s)$ plots (Figs. 4B and 5B and fig. S20B and S24B).

The close similarity between CAP-H2 prometaphase and WT prophase Hi-C, as well as the lack of the second diagonal, allowed us to model CAP-H2 chromosomes as a prophase-like array of a single layer of loops emanating from a flexible, nonhelical scaffold. By systematically varying the loop size and the degree of linear compaction, we obtained excellent agreement with experimental $P(s)$ curves for ~40- to 60-kb loops and a linear density of 15 Mb/μm for all prometaphase time points (Fig. 5, D and E). This linear density is one-third to one-fourth that of WT prometaphase chromosomes (50 to 70 Mb/μm). These simulations indicate that in the absence of condensin II, prometaphase chromosomes form extended prophase-like loop arrays and do not progress to further longitudinal shortening and helical winding.

Condensin I modulates the internal organization of prometaphase helical layers

Cells depleted for CAP-H (fig. S19) seemed to progress through prophase normally: Hi-C data show a rapid loss of compartments and TADs (Fig. 4C and figs. S20C, S22, and S23), and by late prophase, individual chromosomes were discerned by DAPI staining (fig. S21). Deviation from the WT morphogenesis pathway was observed

during prometaphase (i.e., after NEBD), when the bulk of condensin I normally loads in the wild type (fig. S4, B and C). A second diagonal was observed at 30 min, indicating helical winding of the chromatids (Fig. 4C and fig. S20C), but this was located at a genomic distance of ~12 Mb, which in WT cells was only observed at $t = 60$ min. Therefore, the progression to larger helical turns during prometaphase is accelerated in cells lacking CAP-H.

Despite a spiral organization, the loss of condensin I leads to a different loop arrangement and folding, as seen from differences in the $P(s)$ curves: The intralayer arrangement of loops shows a characteristic $P(s) \sim s^{-0.5}$ from 400 kb to ~3 Mb, with $P(s)$ for the $s < 400$ kb region having a different slope, possibly reflecting a different intra-

loop organization. These features are captured well by the coarse-grained model, with 200- to 400-kb loops emanating with correlated angular orientations from a spiral scaffold (Fig. 5G). This loop size agrees well with the sizes of outer loops in the best models for WT chromosomes at $t = 60$ min (Fig. 3H).

When we matched the $t = 30$ min $P(s)$ curve with the simulations of prometaphase chromosomes with helical scaffolds and nested loops, the best match was achieved with either a single layer of 200-kb loops or a nested system of loops, with 400-kb outer loops and 200-kb inner loops (Fig. 5F). Together these results suggest that CAP-H (condensin I) is essential for the formation of short (60- to 80-kb) inner loops but is dispensable for ~200- to 400-kb outer loops

emanating from a helical staircase scaffold. The helical arrangement appears weaker in condensin I–depleted chromosomes, as illustrated by the reduced strength of the second diagonal and reduced peaks in the $P(s)$ plots. One possible reason for this could be the much larger loop sizes in condensin I–depleted chromosomes that may allow larger disorder in their angular arrangement. Taken together, our data obtained with CAP-H– and CAP-H2–depleted cells support the formation of nested loops during prometaphase.

Discussion

We delineate a folding pathway from interphase to metaphase at minute time resolution. Hi-C data reveal a periodic pattern of interactions
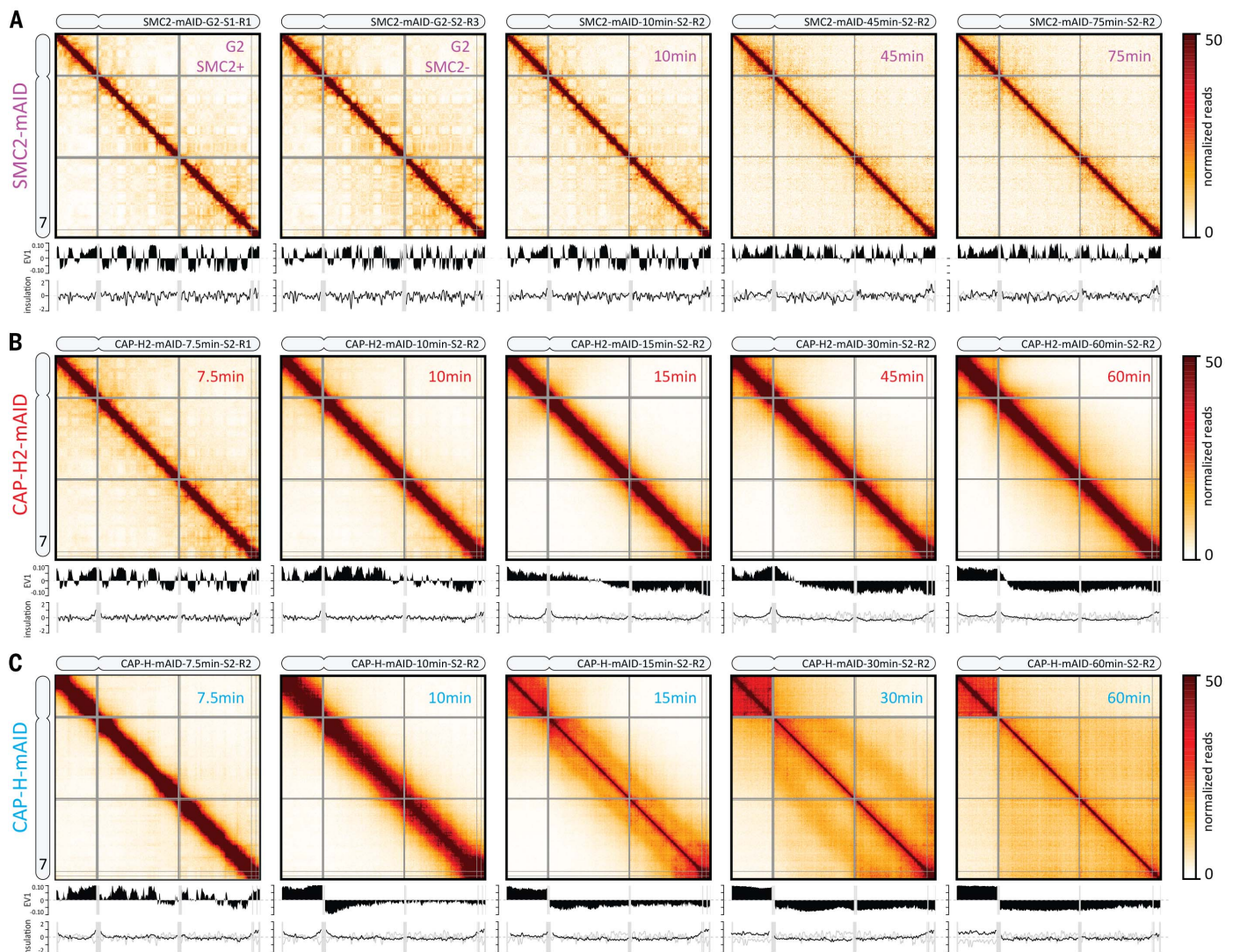
Fig. 4. Defects in chromosome morphogenesis in condensin-depleted cells. (A to C). Hi-C interaction frequency maps (binned at 100 kb) for chromosome 7 at the indicated time points (top right in each heat map) after release from G_2 arrest. The first plot below each Hi-C interaction map displays the compartment signal (eigenvector 1). The bottom graph shows the insulation score (TADs; binned at 50 kb). (A) SMC2-mAID cells were treated with auxin for 3 hours before release from G_2 arrest to deplete SMC2. SMC2+: Hi-C interaction map for G_2-arrested cells before auxin treatment. SMC2−: Hi-C interaction map for G_2-arrested cells after 3 hours of auxin treatment. (B) Hi-C data for CAP-H2–mAID cells treated for 3 hours with auxin before release from G_2 arrest to deplete CAP-H2. (C) Hi-C data for CAP-H–mAID cells treated for 3 hours with auxin before release from G_2 arrest to deplete CAP-H.

that we show to be consistent with a spiral staircase model of mitotic chromosome folding. This model unifies many disparate observations made over the past several decades. We demonstrate that mitotic chromosomes have nested loops formed by differential action of condensin I and II, with condensin II being required for helical coiling of mitotic chromosomes. Finally, we find that condensins are required for the timely loss of the interphase nuclear architecture.

A mitotic chromosome morphogenesis pathway

The data and modeling presented here suggest a chromosome morphogenesis pathway by which cells convert interphase chromosome organization into compacted mitotic chromosomes (Fig. 6). Together with previous observations (*11*), our imaging and Hi-C data, coarse-grained models, and polymer simulations reveal that interphase features such as compartments and TADs are lost within minutes upon entry into prophase, in a condensin-dependent process, and that by late prophase, chromosomes are organized as radial loop arrays. The mechanism by which TADs and compartments are lost is not known, but our data show that condensin is required. Additional contributing factors could include the loss of CTCF and cohesin binding (fig. S4, B and C) and increased levels of loop extrusion that can erase boundaries even when CTCF is still bound (fig. S27). Activation of the mitotic kinase cascade is not sufficient to disassemble
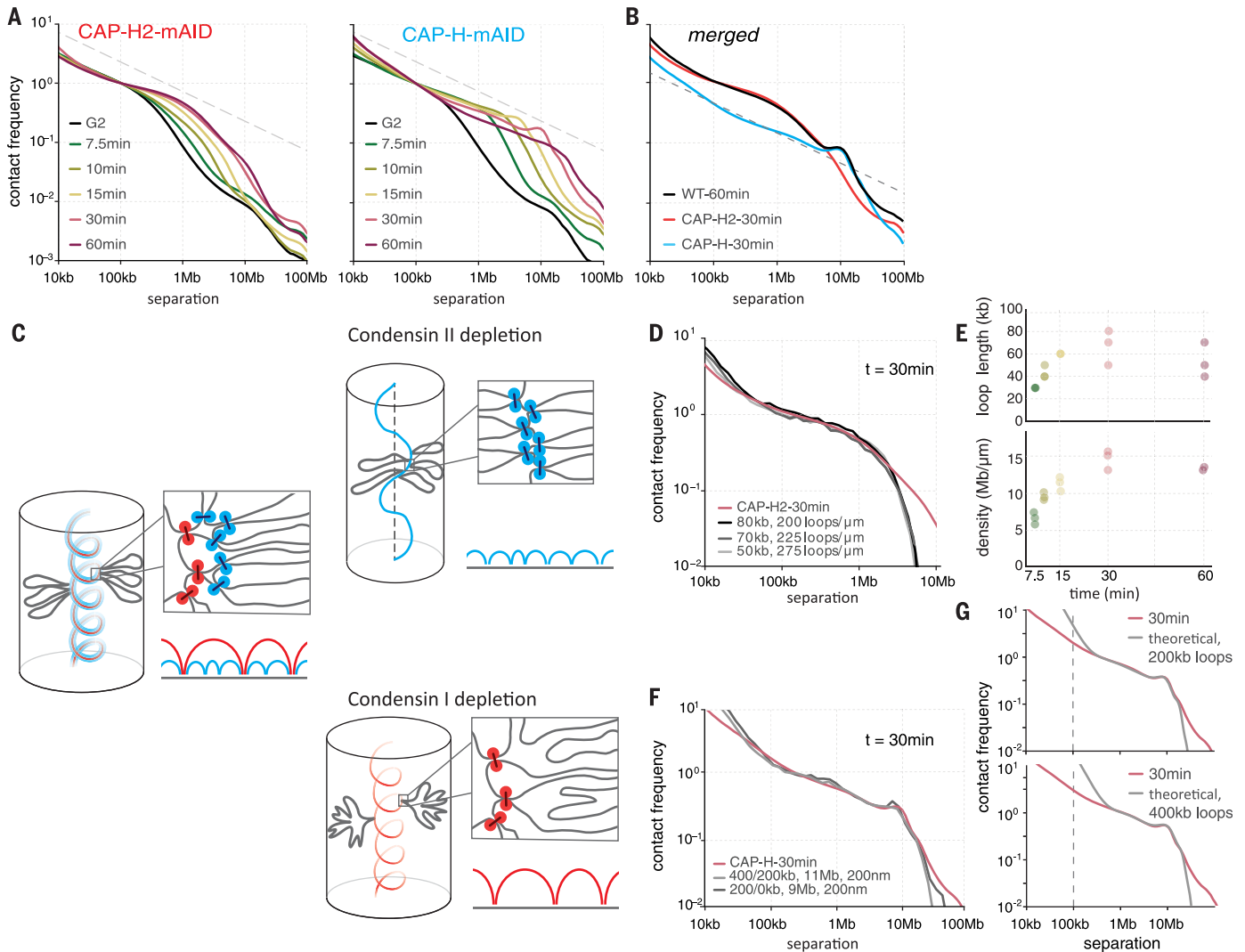
Fig. 5. Distinct roles for condensin I and II in mitotic chromosome formation. (**A**) Genome-wide curves of contact frequency $P(s)$ versus genomic distance s, normalized to unity at $s = 100$ kb. The curves are $P(s)$ derived from Hi-C data obtained from CAP-H2–depleted (left) and CAP-H–depleted (right) cells, at $t = 7$ to 60 min after release from G_2 arrest. Dashed line indicates $P(s) = s^{-0.5}$. (**B**) Overlaid $P(s)$ curves of WT, CAP-H–, and CAP-H2–depleted chromosomes show independent contributions of two condensin complexes to short- and long-distance contacts. (**C**) Polymer models of CAP-H2–depleted (top) and CAP-H–depleted (bottom) chromosomes. (Top) Depletion of CAP-H2 is modeled via removal of outer loops and relaxation of the helix. (Bottom) Depletion of CAP-H is modeled via removal of the inner loops while preserving the helical arrangement of the scaffold. Condensin II loop anchors are shown in red; condensin I loop anchors are shown in blue. (**D**) $P(s)$ derived from late prometaphase CAP-H2–depletion Hi-C experiments (red line) and the three best-fitting polymer models (grayscale lines). The average loop size and linear density of loops along the chromosome axis are indicated. (**E**) Average loop size and linear DNA density of the three best-fitting models of CAP-H2–depleted chromosomes at different time points. (**F**) $P(s)$ derived from late prometaphase CAP-H–depletion Hi-C experiments (red line) and the best-fitting polymer models with and without nested inner loops (grayscale lines). The average size of the outer and inner loops, the length of a helix turn in megabases, and the helical pitch are indicated. (**G**) Best-fitting $P(s)$ predictions by the staircase coarse-grained model for late prometaphase CAP-H–depletion Hi-C experiments at $t = 30$ min after release of G_2 arrest (gray lines). Red lines denote experimental $P(s)$. (Top) Loop size is 200 kb; (bottom) loop size is 400 kb.

Fig. 6. A mitotic chromosome morphogenesis pathway. In prophase, condensin II compacts chromosomes into arrays of consecutive loops and sister chromatids split along their length. The scaffold of condensin II–mediated loop bases is indicated in red. Upon nuclear envelope breakdown and entry into prometaphase, condensin II–mediated loops become increasingly large as they split into smaller ~80-kb loops by condensin I. Chromosomes are shown as arrays of loops. Top, cross section; bottom, side view. (Only inner loops can be observed microscopically. For clarity, loops are indicated as separate entities pointing in one direction, though in reality loops are unstructured and can mix.) The nested arrangements of centrally located condensin II–mediated loop bases and more peripherally located condensin I–mediated loop bases are indicated in red and blue, respectively. During prometaphase, the central scaffold acquires a helical arrangement with loops rotating around the scaffold as steps in a spiral staircase (the helical path of the loops is indicated by arrows). As prometaphase progresses, outer loops grow, the number of loops per turn increases, and chromosomes shorten to form the mature mitotic chromosome.
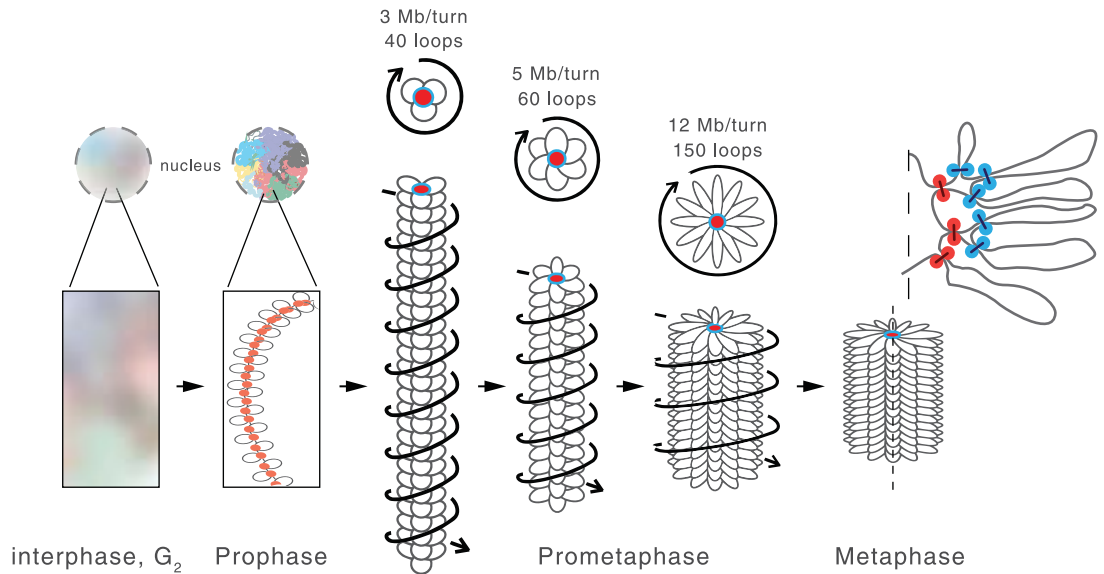
interphase chromatin organization without the action of condensin.

Our models that achieve the best agreement with Hi-C data show that, during prophase, condensin II–dependent loops grow from 30 to 40 kb up to 60 kb in size, leading to a ~twofold increase in linear chromatin density from ~7 to 15 Mb/μm. Condensins at loop bases form a chromosomal scaffold (19, 62), which may be a dynamic rather than static structure, and loops are arranged consecutively along it (one loop every ~5 nm of the axis). The radial arrangement of loops around the central flexible scaffold is not random, with consecutive loops projecting in similar directions; that is, with an angularly correlated arrangement.

Chromosomes shorten along their longitudinal axis and become wider during prometaphase. Our simulations show that condensin II loops continue to grow to 200 to 400 kb by 30 min and 400 to 700 kb by 60 min, accompanied by an increase in the linear chromatin density, which reaches 60 Mb/μm. However, two important reorganizations take place during prometaphase. First, large condensin II–mediated loops are subdivided into smaller 80-kb loops in a condensin I–dependent process, thus producing a nested loop arrangement with ~400-kb outer loops and ~80-kb inner loops. Second, the loop array acquires a helical arrangement as evidenced by the appearance of a second diagonal band in Hi-C maps for all loci and chromosomes. Models show that this helical arrangement of loops can be achieved if the scaffold forms a narrow helical spiral staircase inside an otherwise homogeneous cylindrical chromosome. The radius, height of

each turn (pitch), and number of kilobases per turn of this helix continue to grow through prometaphase, and this growth is somewhat restrained by condensin I. An emerging model of the prometaphase chromosome thus has a central helical scaffold, formed by condensin II (62), that organizes 200- to 400-kb outer loops that are further subdivided into 80-kb condensin I–mediated inner loops to achieve a high volume density.

Chromosomes in DT40 cells range in size from almost 200 Mb to less than 1 Mb. Our Hi-C analysis shows that the organization of prophase and prometaphase chromosomes is largely independent of their length: The size of loops and the amount of DNA per helical turn is the same for all chromosomes larger than 10 to 20 Mb (fig. S11). For the chromosomes that are shorter than one turn of the helix (which together contain <6% of the chicken genome), we do not see the second diagonal in the Hi-C maps, indicating that, as expected, the scaffold is too short and cannot complete a full helical turn. (fig. S11). Simulating the structure of short (<10 to 20 Mb) chromosomes is difficult because most of their chromatin is close to a telomere or a centromere, which may affect its organization, and our models do not describe how DNA is arranged at the tips of the chromosomes.

Comparison to previous and classical studies

Although specific details of this model emerge from an unbiased fitting of models to the data, the emerging organization and its quantitative characteristics agree with earlier studies. First, the 60- to 80-kb sizes of the inner loops are

decidedly similar to values suggested by an extensive survey of the literature (44), measurements from electron microscopy (6, 19), and Hi-C analysis of mitotic HeLa cells (8). Similarly, changes of linear density from prophase to prometaphase in the best models (from 15 to 50 Mb/μm) are consistent with prophase chromosomes being at least twice as long as metaphase chromosomes (11, 61).

Second, helical prometaphase chromosomes have long been observed in certain chromosome preparations (10, 37, 38, 40), and this has led to diverse models for how mitotic chromosomes are folded. Our analysis of Hi-C data indicates that the prometaphase chromosome is organized around a helical central region or scaffold: Loops emanate with helical packing from a centrally located spiral staircase scaffold. Modeling shows that other helical arrangements of loop arrays—for instance, coiling of the entire loop array itself (40, 50, 65, 66)—are not consistent with our Hi-C data.

Our helical scaffold-loop model unifies a range of models and observations made over the years. It explains how a helical chromatin packing arrangement can be achieved while scaffold proteins such as condensins and topoisomerase II are localized centrally (15–17), within a cylindrical chromatid that is not obviously helical when visualized with a DNA dye such as DAPI (67). By late prometaphase, we estimate the height of one helical turn to be ~200 nm, which is also the size of the layer (12-Mb layer at a linear density of 60 Mb/μm) and is consistent with microscope observations suggesting that consecutive genomic loci follow a helical gyre

with a pitch of ~250 nm within the cylindrical shape of chromatids (*68*).

Possible mechanisms

Such loop arrangements can naturally emerge as a result of a loop extrusion process. Loop extrusion has been hypothesized as a mechanism of chromosome compaction (*69*, *70*) and most recently examined by simulations (*25*, *48*, *71*) and supported by single-molecule studies (*72*). In this process, each condensin starts forming a progressively larger loop until it dissociates or stops as it is blocked by neighboring condensins or other DNA-binding proteins. A recent study demonstrated that this process can form an array of consecutive loops (*8*) with condensins forming a central scaffold in the middle of a cylindrical chromosome (*48*), essential features of mitotic chromosomes. Sister chromatids are resolved by late prophase (*11*–*13*), indicating that the formation of loop arrays occurs as sister chromatid arms become separated.

Another aspect of loop extrusion is that loop sizes are established by a dynamic process of condensin exchange, without a need for barrier elements or specific loading sites (*25*). This is consistent with our Hi-C data that suggests that loop bases are not positioned at specific reproducible positions [e.g., scaffold or matrix attachment regions (*73*, *74*)] in a population of cells. Analysis of published ChIP data for SMC2 in mitotic DT40 cells (*45*) shows a low level of condensin binding throughout the genome and only very few loci enriched in condensin binding: Only 289 sites show more than a fivefold enrichment compared with DNA input, and 4617 sites show more than twofold enrichment. These numbers are much lower than the 16,000 inner loops our data and models predict. The condensin-enriched sites show a Hi-C interaction pattern consistent with them being at the bases of loops slightly more frequently than other loci (fig. S13). On the basis of these analyses, we estimate that more than 95% of mitotic loops are not positioned at specific loci.

Simulations show that loop extrusion slowly approaches the steady state by exchanging condensins and gradually increasing loop sizes during this process (*25*). This is consistent with the gradual growth of loops up to 500 kb by slowly-exchanging condensin II, as well as relatively rapid formation of 60- to 80-kb inner loops by the more rapidly-exchanging condensin I (*75*).

The formation of nested loops was critical for our polymer simulations to reproduce prometaphase Hi-C data because only this allowed a higher linear chromatin density. In this architecture, the outer loop bases are located at the central scaffold, whereas the inner, nested loop bases are radially displaced. Our analysis of condensin I or II depletion reveals that condensin II generates outer loops and condensin I generates inner loops. Our simulations reveal that this nested loop arrangement can be explained by the longer half-life of condensin II and the shorter half-life of condensin I on chromatin, as measured by fluorescence recovery after photobleaching (*75*) (movie S1). Nested loops form only in prometaphase, when condensin I gains access to chromatin. Thus, loop extrusion models can explain the nested loop arrangement of condensed mitotic chromosomes.

Why condensin II–based scaffolds acquire helicity only in prometaphase (and not in prophase) is not known, but this could involve interactions with other proteins, such as DNA topoisomerase II alpha or KIF4A. Our estimates of the radius of the prometaphase scaffold (30 to 100 nm) are consistent with a 50-nm length of SMC coiled coils that can interact with each other through HEAT repeats (*76*), which are known for their ability to self-assemble into a helical spiral staircase (*77*). Gradual formation of such a HEAT-mediated staircase and binding of other factors can explain how the pitch and the radius of the helix increase in time.

Mitotic chromatin still condenses in the absence of both condensin I and II, although individualized rod-shaped chromosomes are not formed and cells cannot progress into anaphase. This suggests additional mechanisms by which chromatin becomes condensed during mitosis. Our simulations also show that to achieve agreement with Hi-C data, chromatin should be condensed (computationally analogous to poor solvent conditions), forming densely packed chromatin loops within mitotic chromosomes, akin to the dense packing of chromatin observed in mitotic chromosomes by electron microscopy (*46*, *78*, *79*). The molecular basis for this compaction is not known but may involve mitosis-specific chromatin modifications (*80*, *81*) or active motor proteins such as KIF4A (*82*, *83*).

The chromosome morphogenesis pathway described here, and the identification of distinct architectural roles for condensin I and II in organizing chromosomes as nested loop arrays winding around a helical spiral staircase scaffold within a cylindrical chromatid, can guide future experiments to uncover the molecular mechanisms by which these complexes, and other key components such as topoisomerase II alpha and KIF4A, act in generating, (re)arranging, and condensing chromatin loops to build the mitotic chromosome.

Methods summary

DT40 cell cultures synchronously entering mitosis were analyzed by Hi-C, imaging, and proteomics to determine the structure of chromosomes. Hi-C data were used to quantify chromosome compartmentalization and to derive relationships between contact frequency P and genomic distance s. Coarse-grained models and equilibrium polymer simulations were performed to test models of prophase and prometaphase chromosome organization against Hi-C data and to identify the best-fitting parameters for the size of loops, helical turn and pitch, and linear density (megabases per micrometer of chromosome length). Imaging of chromosome dimensions and condensin localization was carried out to validate model predictions. Cell lines expressing condensin subunits fused to auxin-inducible degron domains were used to efficiently deplete these subunits before cells entered mitosis. Hi-C and imaging analysis were then performed to assess the effects of condensin depletion on mitotic chromosome formation. Detailed procedures for all methods are described in the supplementary materials.

REFERENCES AND NOTES

1. J. R. Dixon et al., Topological domains in mammalian genomes identified by analysis of chromatin interactions. Nature **485**, 376–380 (2012). doi: 10.1038/nature11082; pmid: 22495300
2. E. P. Nora et al., Spatial partitioning of the regulatory landscape of the X-inactivation centre. Nature **485**, 381–385 (2012). doi: 10.1038/nature11049; pmid: 22495304
3. E. Lieberman-Aiden et al., Comprehensive mapping of long-range interactions reveals folding principles of the human genome. Science **326**, 289–293 (2009). doi: 10.1126/science.1181369; pmid: 19815776
4. S. S. Rao et al., A 3D map of the human genome at kilobase resolution reveals principles of chromatin looping. Cell **159**, 1665–1680 (2014). doi: 10.1016/j.cell.2014.11.021; pmid: 25497547
5. A. Sanyal, B. R. Lajoie, G. Jain, J. Dekker, The long-range interaction landscape of gene promoters. Nature **489**, 109–113 (2012). doi: 10.1038/nature11279; pmid: 22955621
6. W. C. Earnshaw, U. K. Laemmli, Architecture of metaphase chromosomes and chromosome scaffolds. J. Cell Biol. **96**, 84–93 (1983). doi: 10.1083/jcb.96.1.84; pmid: 6826654
7. M. P. Marsden, U. K. Laemmli, Metaphase chromosome structure: Evidence for a radial loop model. Cell **17**, 849–858 (1979). doi: 10.1016/0092-8674(79)90325-8; pmid: 487432
8. N. Naumova et al., Organization of the mitotic chromosome. Science **342**, 948–953 (2013). doi: 10.1126/science.1236083; pmid: 24200812
9. T. Nagano et al., Cell-cycle dynamics of chromosomal organization at single-cell resolution. Nature **547**, 61–67 (2017). doi: 10.1038/nature23001; pmid: 28682332
10. Y. Ohnuki, Structure of chromosomes. I. Morphological studies of the spiral structure of human somatic chromosomes. Chromosoma **25**, 402–428 (1968). doi: 10.1007/BF02327721; pmid: 4894149
11. Z. Liang et al., Chromosomes progress to metaphase in multiple discrete steps via global compaction/expansion cycles. Cell **161**, 1124–1137 (2015). doi: 10.1016/j.cell.2015.04.030; pmid: 26000485
12. K. Nagasaka, M. J. Hossain, M. J. Roberti, J. Ellenberg, T. Hirota, Sister chromatid resolution is an intrinsic part of chromosome organization in prophase. Nat. Cell Biol. **18**, 692–699 (2016). doi: 10.1038/ncb3353; pmid: 27136266
13. L. L. Moore, M. B. Roth, HCP-4, a CENP-C-like protein in Caenorhabditis elegans, is required for resolution of sister centromeres. J. Cell Biol. **153**, 1199–1208 (2001). doi: 10.1083/jcb.153.6.1199; pmid: 11402064
14. K. W. Adolphs, S. M. Cheng, J. R. Paulson, U. K. Laemmli, Isolation of a protein scaffold from mitotic HeLa cell chromosomes. Proc. Natl. Acad. Sci. U.S.A. **74**, 4937–4941 (1977). doi: 10.1073/pnas.74.11.4937; pmid: 270727
15. W. C. Earnshaw, M. M. Heck, Localization of topoisomerase II in mitotic chromosomes. J. Cell Biol. **100**, 1716–1725 (1985). doi: 10.1083/jcb.100.5.1716; pmid: 2985626
16. S. M. Gasser, U. K. Laemmli, The organisation of chromatin loops: Characterization of a scaffold attachment site. EMBO J. **5**, 511–518 (1986). pmid: 16453673
17. Y. Saitoh, U. K. Laemmli, Metaphase chromosome structure: Bands arise from a differential folding path of the highly AT-rich scaffold. Cell **76**, 609–622 (1994). doi: 10.1016/0092-8674(94)90502-9; pmid: 7510215
18. K. Samejima et al., Mitotic chromosomes are compacted laterally by KIF4 and condensin and axially by topoisomerase IIα. J. Cell Biol. **199**, 755–770 (2012). doi: 10.1083/jcb.201202155; pmid: 23166350
19. J. R. Paulson, U. K. Laemmli, The structure of histone-depleted metaphase chromosomes. Cell **12**, 817–828 (1977). doi: 10.1016/0092-8674(77)90280-X; pmid: 922894
20. M. Okada, T. Hori, T. Fukagawa, The DT40 system as a tool for analyzing kinetochore assembly. Subcell. Biochem. **40**, 91–106 (2006). pmid: 17623902
21. A. C. Bishop et al., Design of allele-specific inhibitors to probe protein kinase signaling. Curr. Biol. **8**,

257–266 (1998). doi: 10.1016/S0960-9822(98)70198-8; pmid: 9501066

22. H. Hochegger *et al.*, An essential role for Cdk1 in S phase control is revealed via chemical genetics in vertebrate cells. *J. Cell Biol.* **178**, 257–268 (2007). doi: 10.1083/jcb.200702034; pmid: 17635936

23. K. Samejima *et al.*, A promoter-hijack strategy for conditional shutdown of multiply spliced essential cell cycle genes. *Proc. Natl. Acad. Sci. U.S.A.* **105**, 2457–2462 (2008). doi: 10.1073/pnas.0712083105; pmid: 18263736

24. G. Fudenberg *et al.*, Formation of chromosomal domains by loop extrusion. *Cell Reports* **15**, 2038–2049 (2016). doi: 10.1016/j.celrep.2016.04.085; pmid: 27210764

25. A. Goloborodko, J. F. Marko, L. A. Mirny, Chromosome compaction by active loop extrusion. *Biophys. J.* **110**, 2162–2168 (2016). doi: 10.1016/j.bpj.2016.02.041; pmid: 27224481

26. A. J. Holland, D. Fachinetti, J. S. Han, D. W. Cleveland, Inducible, reversible system for the rapid and complete degradation of proteins in mammalian cells. *Proc. Natl. Acad. Sci. U.S.A.* **109**, E3350–E3357 (2012). doi: 10.1073/pnas.1216880109; pmid: 23150568

27. K. Nishimura, T. Fukagawa, H. Takisawa, T. Kakimoto, M. Kanemaki, An auxin-based degron system for the rapid depletion of proteins in nonplant cells. *Nat. Methods* **6**, 917–922 (2009). doi: 10.1038/nmeth.1401; pmid: 19915560

28. E. Sonoda, M. Takata, Y. M. Yamashita, C. Morrison, S. Takeda, Homologous DNA recombination in vertebrate cells. *Proc. Natl. Acad. Sci. U.S.A.* **98**, 8388–8394 (2001). doi: 10.1073/pnas.111006398; pmid: 11459980

29. S. D. Georgatos, A. Pyrpasopoulou, P. A. Theodoropoulos, Nuclear envelope breakdown in mammalian cells involves stepwise lamina disassembly and microtubule-drive deformation of the nuclear membrane. *J. Cell Sci.* **110**, 2129–2140 (1997). pmid: 9378763

30. I. C. Waizenegger, S. Hauf, A. Meinke, J. M. Peters, Two distinct pathways remove mammalian cohesin from chromosome arms in prophase and from centromeres in anaphase. *Cell* **103**, 399–410 (2000). doi: 10.1016/S0092-8674(00)00132-X; pmid: 11081627

31. A. Losada, M. Hirano, T. Hirano, Cohesin release is required for sister chromatid resolution, but not for condensin-mediated compaction, at the onset of mitosis. *Genes Dev.* **16**, 3004–3016 (2002). doi: 10.1101/gad.249202; pmid: 12464631

32. E. Crane *et al.*, Condensin-driven remodelling of X chromosome topology during dosage compensation. *Nature* **523**, 240–244 (2015). doi: 10.1038/nature14450; pmid: 26030525

33. M. Imakaev *et al.*, Iterative correction of Hi-C data reveals hallmarks of chromosome organization. *Nat. Methods* **9**, 999–1003 (2012). doi: 10.1038/nmeth.2148; pmid: 22941365

34. S. Abe *et al.*, The initial phase of chromosome condensation requires Cdk1-mediated phosphorylation of the CAP-D3 subunit of condensin II. *Genes Dev.* **25**, 863–874 (2011). doi: 10.1101/gad.2016411; pmid: 21498573

35. W. Schwarzer *et al.*, Two independent modes of chromatin organization revealed by cohesin removal. *Nature* **551**, 51–56 (2017). pmid: 29094699

36. E. P. Nora *et al.*, Targeted degradation of CTCF decouples local insulation of chromosome domains from genomic compartmentalization. *Cell* **169**, 930–944.e22 (2017). doi: 10.1016/j.cell.2017.05.004; pmid: 28525758

37. J. Baranetzky, Die Kerntheilung in den Pollenmutterzellen einiger Tradescantien. *Bot. Zeitung* **38**, 281–296 (1880).

38. Y. Kuwada, Chromosome structure: A critical review. *Cytologia* **10**, 213–256 (1939). doi: 10.1508/cytologia.10.213

39. C. L. Woodcock, L. L. Frado, J. B. Rattner, The higher-order structure of chromatin: Evidence for a helical ribbon arrangement. *J. Cell Biol.* **99**, 42–52 (1984). doi: 10.1083/jcb.99.1.42; pmid: 6736132

40. E. B. de la Tour, U. K. Laemmli, The metaphase scaffold is helically folded: Sister chromatids have predominantly opposite helical handedness. *Cell* **55**, 937–944 (1988). doi: 10.1016/0092-8674(88)90239-5; pmid: 2849511

41. J. M. Craig, W. A. Bickmore, Chromosome bands—Flavours to savour. *BioEssays* **15**, 349–354 (1993). doi: 10.1002/bies.950150510; pmid: 8343145

42. J. Paturej, S. S. Sheiko, S. Panyukov, M. Rubinstein, Molecular structure of bottlebrush polymers in melts. *Sci. Adv.* **2**, e1601478 (2016). doi: 10.1126/sciadv.1601478 pmid: 28861466

43. J. F. Marko, E. D. Siggia, Polymer models of meiotic and mitotic chromosomes. *Mol. Biol. Cell* **8**, 2217–2231 (1997). doi: 10.1091/mbc.8.11.2217; pmid: 9362064

44. K. J. Pienta, D. S. Coffey, A structural analysis of the role of the nuclear matrix and DNA loops in the organization of the nucleus and chromosome. *J. Cell Sci. Suppl.* **1984**, 123–135 (1984). doi: 10.1242/jcs.1984.Supplement_1.9; pmid: 6397469

45. J. H. Kim *et al.*, Condensin I associates with structural and gene regulatory regions in vertebrate chromosomes. *Nat. Commun.* **4**, 2537 (2013). doi: 10.1038/ncomms3537; pmid: 24088984

46. H. D. Ou *et al.*, ChromEMT: Visualizing 3D chromatin structure and compaction in interphase and mitotic cells. *Science* **357**, eaag0025 (2017). doi: 10.1126/science.aag0025; pmid: 28751582

47. Y. Nishino *et al.*, Human mitotic chromosomes consist predominantly of irregularly folded nucleosome fibres without a 30-nm chromatin structure. *EMBO J.* **31**, 1644–1653 (2012). doi: 10.1038/emboj.2012.35; pmid: 22343941

48. A. Goloborodko, M. V. Imakaev, J. F. Marko, L. Mirny, Compaction and segregation of sister chromatids via active loop extrusion. *eLife* **5**, e14864 (2016). doi: 10.7554/eLife.14864; pmid: 27192037

49. D. G. Booth *et al.*, 3D-CLEM reveals that a major portion of mitotic chromosomes is not chromatin. *Mol. Cell* **64**, 790–802 (2016). doi: 10.1016/j.molcel.2016.10.009; pmid: 27840028

50. J. B. Rattner, C. C. Lin, Radial loops and helical coils coexist in metaphase chromosomes. *Cell* **42**, 291–296 (1985). doi: 10.1016/S0092-8674(85)80124-0; pmid: 4016953

51. B. D. Hughes, *Random Walks and Random Environments, Volume I: Random Walks* (Clarendon Press, 1995).

52. T. Hirota, D. Gerlich, B. Koch, J. Ellenberg, J.-M. Peters, Distinct functions of condensin I and II in mitotic chromosome assembly. *J. Cell Sci.* **117**, 6435–6445 (2004). doi: 10.1242/jcs.01604; pmid: 15572404

53. T. Ono, Y. Fang, D. L. Spector, T. Hirano, Spatial and temporal regulation of condensins I and II in mitotic chromosome assembly in human cells. *Mol. Biol. Cell* **15**, 3296–3308 (2004). doi: 10.1091/mbc.E04-03-0242; pmid: 15146063

54. D. F. Hudson, P. Vagnarelli, R. Gassmann, W. C. Earnshaw, Condensin is required for nonhistone protein assembly and structural integrity of vertebrate mitotic chromosomes. *Dev. Cell* **5**, 323–336 (2003). doi: 10.1016/S1534-5807(03)00199-0; pmid: 12919682

55. S. Ohta *et al.*, The protein composition of mitotic chromosomes determined using multiclassifier combinatorial proteomics. *Cell* **142**, 810–821 (2010). doi: 10.1016/j.cell.2010.07.047; pmid: 20813266

56. S. Ohta *et al.*, Proteomics analysis with a nano random forest approach reveals novel functional interactions regulated by SMC complexes on mitotic chromosomes. *Mol. Cell. Proteomics* **15**, 2802–2818 (2016). doi: 10.1074/mcp.M116.057885; pmid: 27231315

57. K. Samejima *et al.*, Rapid degradation of condensins and 3D-EM reveal chromatin volume is uncoupled from chromosome architecture in mitosis. *J. Cell Sci.* 10.1242/jcs.210187 (2018). doi: 10.1242/jcs.210187

58. G. Kustatscher, K. L. H. Wills, C. Furlan, J. Rappsilber, Chromatin enrichment for proteomics. *Nat. Protoc.* **9**, 2090–2099 (2014). doi: 10.1038/nprot.2014.142; pmid: 25101823

59. M. Yanagida, Clearing the way for mitosis: Is cohesin a target? *Nat. Rev. Mol. Cell Biol.* **10**, 489–496 (2009). doi: 10.1038/nrm2712; pmid: 19491928

60. T. Ono *et al.*, Differential contributions of condensin I and condensin II to mitotic chromosome architecture in vertebrate cells. *Cell* **115**, 109–121 (2003). doi: 10.1016/S0092-8674(03)00724-4; pmid: 14532007

61. L. C. Green *et al.*, Contrasting roles of condensin I and condensin II in mitotic chromosome formation. *J. Cell Sci.* **125**, 1591–1604 (2012). doi: 10.1242/jcs.097790; pmid: 22344259

62. K. Shintomi *et al.*, Mitotic chromosome assembly despite nucleosome depletion in *Xenopus* egg extracts. *Science* **356**, 1284–1287 (2017). doi: 10.1126/science.aam9702; pmid: 28522692

63. K. Shintomi, T. Hirano, The relative ratio of condensin I to II determines chromosome shapes. *Genes Dev.* **25**, 1464–1469 (2011). doi: 10.1101/gad.2060311; pmid: 21715560

64. T. Zhang *et al.*, Condensin I and II behaviour in interphase nuclei and cells undergoing premature chromosome condensation. *Chromosome Res.* **24**, 243–269 (2016). doi: 10.1007/s10577-016-9519-7; pmid: 27008552

65. A. S. Belmont, J. W. Sedat, D. A. Agard, A three-dimensional approach to mitotic chromosome structure: Evidence for a complex hierarchical organization. *J. Cell Biol.* **105**, 77–92 (1987). doi: 10.1083/jcb.105.1.77; pmid: 3112167

66. A. S. Belmont, S. Dietzel, A. C. Nye, Y. G. Strukov, T. Tumbar, Large-scale chromatin structure and function. *Curr. Opin. Cell Biol.* **11**, 307–311 (1999). doi: 10.1016/S0955-0674(99)80041-6; pmid: 10395564

67. K. Maeshima, U. K. Laemmli, A two-step scaffolding model for mitotic chromosome assembly. *Dev. Cell* **4**, 467–480 (2003). doi: 10.1016/S1534-5807(03)00092-3; pmid: 12689587

68. Y. G. Strukov, Y. Wang, A. S. Belmont, Engineered chromosome regions with altered sequence composition demonstrate hierarchical large-scale folding within metaphase chromosomes. *J. Cell Biol.* **162**, 23–35 (2003). doi: 10.1083/jcb.200303098; pmid: 12835314

69. K. Nasmyth, Disseminating the genome: Joining, resolving, and separating sister chromatids during mitosis and meiosis. *Annu. Rev. Genet.* **35**, 673–745 (2001). doi: 10.1146/annurev.genet.35.102401.091334; pmid: 11700297

70. A. D. Riggs, DNA methylation and late replication probably aid cell memory, and type I DNA reeling could aid chromosome folding and enhancer function. *Philos. Trans. R. Soc. London Ser. B* **326**, 285–297 (1990). doi: 10.1098/rstb.1990.0012; pmid: 1968665

71. E. Alipour, J. F. Marko, Self-organization of domain structures by DNA-loop-extruding enzymes. *Nucleic Acids Res.* **40**, 11202–11212 (2012). doi: 10.1093/nar/gks925; pmid: 23074191

72. T. Terakawa *et al.*, The condensin complex is a mechanochemical motor that translocates along DNA. *Science* **358**, 672–676 (2017). doi: 10.1126/science.aan6516; pmid: 28882993

73. J. Mirkovitch, S. M. Gasser, U. K. Laemmli, Scaffold attachment of DNA loops in metaphase chromosomes. *J. Mol. Biol.* **200**, 101–109 (1988). doi: 10.1016/0022-2836(88)90336-1; pmid: 3132557

74. P. N. Cockerill, W. T. Garrard, Chromosomal loop anchorage of the kappa immunoglobulin gene occurs next to the enhancer in a region containing topoisomerase II sites. *Cell* **44**, 273–282 (1986). doi: 10.1016/0092-8674(86)90761-0; pmid: 3002631

75. D. Gerlich, T. Hirota, B. Koch, J.-M. Peters, J. Ellenberg, Condensin I stabilizes chromosomes mechanically through a dynamic interaction in live cells. *Curr. Biol.* **16**, 333–344 (2006). doi: 10.1016/j.cub.2005.12.040; pmid: 16488867

76. S. H. Yoshimura, T. Hirano, HEAT repeats - versatile arrays of amphiphilic helices working in crowded environments? *J. Cell Sci.* **129**, 3963–3970 (2016). pmid: 27802131

77. B. Kobe *et al.*, Turn up the HEAT. *Structure* **7**, R91–R97 (1999). doi: 10.1016/S0969-2126(99)80060-4; pmid: 10378263

78. E. Robbins, N. K. Gonatas, The ultrastructure of a mammalian cell during the mitotic cycle. *J. Cell Biol.* **21**, 429–463 (1964). doi: 10.1083/jcb.21.3.429; pmid: 14189913

79. M. Eltsov, K. M. Maclellan, K. Maeshima, A. S. Frangakis, J. Dubochet, Analysis of cryo-electron microscopy images does not support the existence of 30-nm chromatin fibers in mitotic chromosomes in situ. *Proc. Natl. Acad. Sci. U.S.A.* **105**, 19732–19737 (2008). doi: 10.1073/pnas.0810057105; pmid: 19064912

80. B. J. Wilkins *et al.*, A cascade of histone modifications induces chromatin condensation in mitosis. *Science* **343**, 77–80 (2014). doi: 10.1126/science.1244508; pmid: 24385627

81. A. Zhiteneva *et al.*, Mitotic post-translational modifications of histones promote chromatin compaction in vitro. *Open Biol.* **7**, 170076 (2017). doi: 10.1098/rsob.170076; pmid: 28903997

82. M. Mazumdar, S. Sundareshan, T. Misteli, Human chromokinesin KIF4A functions in chromosome condensation and segregation. *J. Cell Biol.* **166**, 613–620 (2004). doi: 10.1083/jcb.200401142; pmid: 15326200

83. M. Takahashi, T. Wakai, T. Hirota, Condensin I-mediated mitotic chromosome assembly requires association with chromokinesin KIF4A. *Genes Dev.* **30**, 1931–1936 (2016). doi: 10.1101/gad.282855.116; pmid: 27633014

84. A. Maritan, C. Micheletti, A. Trovato, J. R. Banavar, Optimal shapes of compact strings. *Nature* **406**, 287–290 (2000). doi: 10.1038/35018538; pmid: 10917526

SUPPLEMENTARY MATERIALS

www.sciencemag.org/content/359/6376/eaao6135/suppl/DC1
Materials and Methods
Figs. S1 to S27
Tables S1 to S4
References (85–98)
Movie S1

10 August 2017; accepted 9 January 2018
Published online 18 January 2018
10.1126/science.aao6135

Science

A pathway for mitotic chromosome formation

Johan H. Gibcus, Kumiko Samejima, Anton Goloborodko, Itaru Samejima, Natalia Naumova, Johannes Nuebler, Masato T. Kanemaki, Linfeng Xie, James R. Paulson, William C. Earnshaw, Leonid A. Mirny and Job Dekker

Tracking mitotic chromosome formation

How cells pack DNA into fully compact, rod-shaped chromosomes during mitosis has fascinated cell biologists for more than a century. Gibcus *et al.* delineated the conformational transition trajectory from interphase chromatin to mitotic chromosomes minute by minute during the cell cycle. The mitotic chromosome is organized in a spiral staircase architecture in which chromatin loops emanate radially from a centrally located helical scaffold. The molecular machines condensin I and II play distinct roles in these processes: Condensin II is essential for helical winding, whereas condensin I modulates the organization within each helical turn.

Science, this issue p. eaao6135

ARTICLE TOOLS	http://science.sciencemag.org/content/359/6376/eaao6135
SUPPLEMENTARY MATERIALS	http://science.sciencemag.org/content/suppl/2018/01/17/science.aao6135.DC1
REFERENCES	This article cites 97 articles, 40 of which you can access for free http://science.sciencemag.org/content/359/6376/eaao6135#BIBL
PERMISSIONS	http://www.sciencemag.org/help/reprints-and-permissions

Use of this article is subject to the Terms of Service